Article

JOURNAL OF COMPOSITE MATERIALS

Journal of Composite Materials
2014, Vol. 48(11) 1337–1346

DOI: 10.1177/0021998313485309
jcm.sagepub.com

SAGE

In-plane compression of hollow composite pyramidal lattice sandwich columns

Sha Yin[1], Linzhi Wu[1] and Steven Nutt[2]

Abstract

Composite lattice structures can be regarded as hierarchical when trusses have their own structure (e.g. different stacking sequences are incorporated). In this study, hollow composite pyramidal lattice sandwich structures in end compression were analyzed, measured and evaluated with respect to the designable properties of sandwich cores, such as relative density and truss stacking sequence. Collapse mechanism charts were constructed for both component elements and sandwich columns to illustrate the influence of structural geometries and properties of composite pyramidal lattice cores on failure modes. Operative failure modes were identified and the analytical models were shown to be accurate when compared to the measured response. The minimum weight design for the hollow composite pyramidal lattice sandwich column in end compression was carried out and the structural efficiency was also discussed.

Keywords

Carbon fiber, sandwich structures, lattice materials, collapse mechanism map, minimum weight design

Introduction

Sandwich panels comprising thin face sheets separated by a thick, low-density core are widely used in weight-sensitive structural applications. Common core materials range from stochastic foams, which tend to be relatively low cost and low performance, when compared to periodic honeycombs, which tend to be higher cost and higher performance. In addition, lattice materials are being developed for sandwich cores, generally in plate-like or truss-like configurations. Truss-based lattice topologies (e.g. tetrahedral, pyramidal and Kagome lattice structures) are stretch-dominated, open structures well-suited to multifunctional applications.[1] Such lattice materials can be produced from traditional materials, yielding exceptional performance. For example, metallic lattice cores that feature quasi-static[2–4] and dynamic properties[5–8] competitive with high-performance honeycomb cores have been developed.

In recent years, composite lattices have been developed with optimal topologies to fill gaps in the material property space by exploiting the superior specific properties of composites. These structures have been produced using different methods, including hot press molding,[9–11] thermal expansion molding[12] and interlocking.[13,14] Using the thermal expansion molding technique, we have produced hollow composite pyramidal lattice (CPL) sandwich panels.[12] The structural integrity of the panels can be greatly enhanced by embedding the composite truss ends into the face sheets. Hollow CPL cores are stronger and stiffer than equivalent-weight structures with solid struts, and exhibit exceptional energy absorption capacity.[12] Moreover, the open volume within the hollow trusses provides an opportunity to introduce additional function(s) without significantly changing quasi-static structural properties.[15] The exceptional properties of sandwich structures based on hollow CPLs motivate the further investigation of the response to different modes of loading, such as edgewise compression.[16,17]

[1]Center for Composite Materials, Harbin Institute of Technology, Harbin, China
[2]Department of Chemical Engineering and Materials Science, University of Southern California, Los Angeles, CA, USA

Corresponding author:
Linzhi Wu, Center for Composite Materials, Harbin Institute of Technology, Harbin 150001, China.
Email: wlz@hit.edu.cn

In contrast to solid truss CPLs that comprised solely of axial fibers,[9–11] hollow CPL cores here feature hoop fibers. Because the laminate architecture constitutes one type of structural hierarchy as described by Lakes,[18] another level of hierarchy can be introduced in composite lattice materials where the trusses consist of plies of different orientations assembled in laminated shells. Accordingly, we can term composite lattice materials hierarchical. Previous reports[9,19] describing the compressive properties of composite sandwich structures with lattice core mainly showed the effect of designable properties of face sheets (e.g. stacking sequences) on failure mechanism, but ignored the possibility of designing lattice cores. The scope of the present study encompasses analysis and experiments about hollow CPL sandwich structures in end-compression, focusing on the deformation behavior of sandwich cores and their designable characteristic effect (introduced by hierarchy of parent composites) on structural performance. The minimum weight design is also carried out.

Analysis

The problem considered is a sandwich column subjected to end compression, as depicted in Figure 1(a). The geometry of a representative unit cell is sketched in Figure 1(b), and consists of a hollow CPL core and two composite face sheets. The relative density $\bar{\rho}_h$ can be expressed as

$$\bar{\rho}_h = \frac{\pi\left(d_o^2 - d_i^2\right)}{\sin\omega\left(\sqrt{2}l_1\cos\omega + 2l_2\right)^2} \tag{1}$$

where d_o and d_i are the outer and inner diameters of hollow trusses, l_1 is the truss length, ω is the inclination angle between the truss members and the base of the unit cell, and l_2 represents the spacing at the pyramidal node.

For axial compression of a laminated column or tube, both Euler buckling and crushing are possible failure modes, while for hollow CPL sandwich columns end-loaded in compression, at least four competing failure modes must be considered, as portrayed in Figure 2. Analytical models for the failure modes shown in Figure 2 have been reported previously for solid truss CPL sandwich columns,[9] and the predictions for failure modes of the hollow CPL sandwich panels are similarly derived in the Appendix.

The load states of the hollow CPL core are analyzed for each failure mode and are included in Figure 2. Once the face sheet bends, the forces in the trusses are non-zero, as expected. In the following section, failure mechanism maps are constructed for both the component elements and the hollow CPL sandwich column.

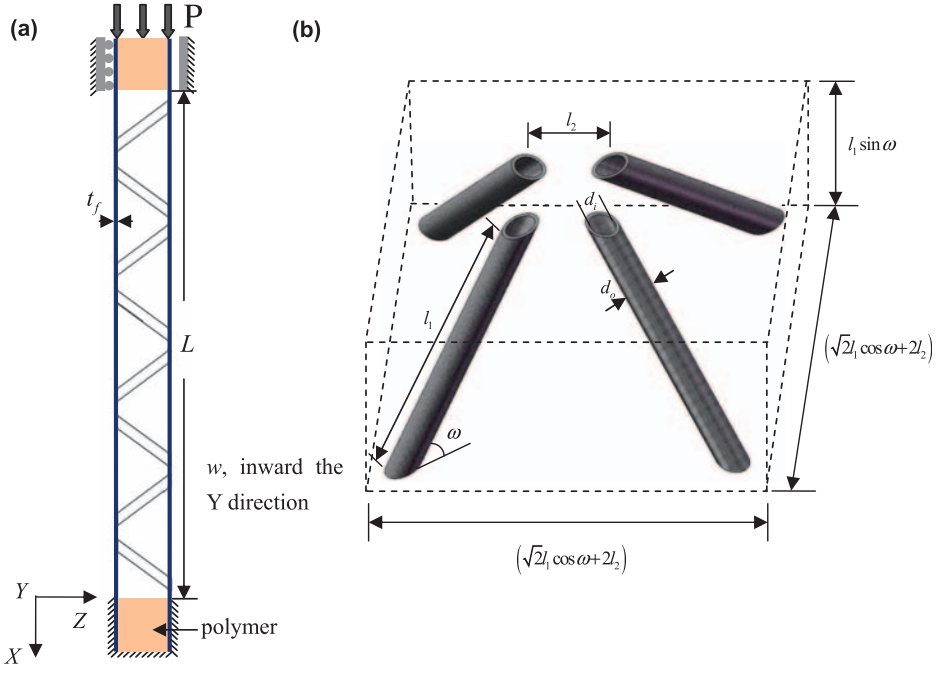

Figure 1. (a) Schematic illustration of an end-clamped second-order hollow composite pyramidal core sandwich column under axial compression; (b) geometries of the hollow CPL core.
CPL: composite pyramidal lattice.

Failure mechanism maps of composite elements in end compression

We consider first an end-clamped flat laminate of length L, width w and thickness t_f subjected to axial compression, causing failure by either buckling or crushing. Note that the possible micro-failure modes for laminates include matrix crushing, fiber buckling, fiber–matrix shear failure, and delamination. The buckling load is given by $P_f = 4\pi^2 D_f / L^2$, where $D_f = \frac{1}{2} E_f^{eq} w t_f^3$ is the equivalent flexural rigidity of the laminate, and E_f^{eq} is the equivalent elastic modulus of the laminate deduced from classical laminate theory.[20] A competing failure mode is face sheet crushing (FC), for which the associated strength is denoted as σ_f. The compressive modulus and failure strength will vary with the laminate stacking sequence of each of these composite elements, and these values are summarized in Table 1.[9] From this information, a failure mechanism map can be constructed, as shown in Figure 3(a). The three vertical lines represent transition values between buckling and fracture for three different stacking sequences illustrated in the figure. The failure mode depends primarily on the geometrical parameter t_f/L (thickness-to-length ratio), but is also affected by σ_f/E_f^{eq}, particularly for small σ_f/E_f^{eq} ratios. However, for carbon fiber face sheets commonly used in sandwich constructions ($t_f/L < 0.025$), Euler buckling of the face sheets is the most likely failure mode (Figure 3(a)), and thus the change of σ_f/E_f^{eq} achieved by varying the laminate stacking sequence has little effect on the failure mode.

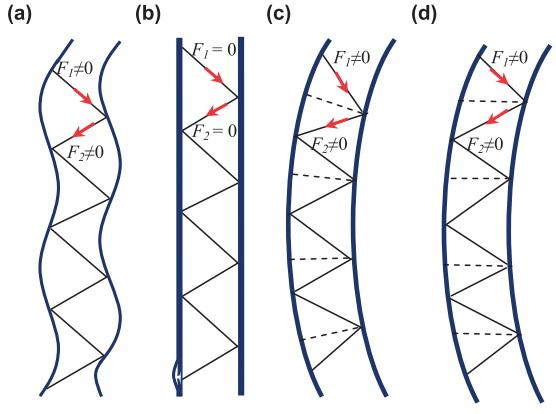

Figure 2. Failure modes of hollow CPL sandwich columns subjected to edgewise compression combined with the load state of the hollow CPL core: (a) face sheet wrinkling; (b) face sheet crushing; (c) Euler macro-buckling; (d) core shear macro-buckling. F_1 and F_2 represent forces in the two pairs of hollow trusses of hollow CPL, respectively.
CPL: composite pyramidal lattice.

Similarly, a failure mechanism map can be constructed for a composite tube loaded in axial compression, using the parameters given in Table 1, where E_f^{eq} and σ_{sh} are the equivalent modulus and fracture strength of composite tubes. The map is shown in Figure 3(b), and includes the domains for Euler buckling and fracture. Similarly, the three colored lines represent the transition between buckling and fracture for three stacking sequences of hollow trusses in Table 1 when σ_{sh}/E_{sh}^{eq} increases. However, as shown in Figure 3(b), if the selected d_o/l_1 and d_i/l_1 ratios lie within the transition region (between the black curve and the blue one), the failure mode may shift between Euler buckling and fracture.

Failure mechanism maps for sandwich columns in end compression

Collapse mechanism maps for the edgewise compressive failure of a second-order CPL sandwich column are shown in Figure 4. Here, the prescribed core geometries include $d_o/l_1 = 0.3$ and inclination angle $\omega = 45^\circ$. The maps shown in Figure 4(a) to (c) are constructed as functions of face sheet parameters t_f/l_1 and L/l_1 for different truss parameters ($d_i/l_1 = 0.27$, 0.225 and 0.15). The compressive properties of face sheets are based on the measured values for ([0/90/0]) laminates given in experimental section below, while the values for hollow trusses are taken from Table 1. The boundaries on the map are obtained by equating the collapse loads for different failure modes, and shift for the three different values of d_i/l_1. Note that the collapse mechanism maps depend strongly on truss parameter, d_i/l_1. This behavior is attributed to the dependence of shear stiffness of the hollow CPL on the relative density $\bar{\rho}_h(d_i)$ and the elastic modulus of the composite tube E_{sh}^{eq} (equation (9) in the Appendix). Because the core density is relatively low ($d_i/l_1 = 0.27$), face sheet crushing is unlikely, and shear buckling is expected to dominate in most of the design space as shown in Figure 4(a). However, as the core density increases ($d_i/l_1 = 0.225$ or 0.15), sandwich panels may be susceptible to any of the four failure mechanism (Figure 4(b) and (c)). Note that the domain size for face wrinkling (FW) is the same for $d_i/l_1 = 0.225$ and 0.15, although other domain sizes vary substantially. Such collapse mechanism maps can be used for different purposes. For example, they can guide specimen designs to probe the limits of different failure modes and test the robustness of the analytical models presented in the Appendix.

We also explore the influence of E_{sh}^{eq} on the failure mode location by varying the stacking sequence. For this purpose, we construct a second kind of failure map in which we plot failure modes as functions of t_f/l_1 and d_i/l_1 for a given $L/l_1 = 0$, as shown in Figure 4(d).

Table 1. Mechanical properties of composite elements.

Laminated face sheet				Stacking sequence	E_f^{eq} (GPa)	σ_f (MPa)
				[0/90/90/0]	59.2	534
				[0/+45/−45/90]	22.5	317
				[0/90/0]	76.1	646
Laminated shell (hollow truss)	d_o (mm)	d_i (mm)	$\bar{\rho}_h$ (%)	Stacking sequence	E_{sh}^{eq} (GPa)	σ_{sh} (MPa)
	6	5.4	1.07	[(0,90)]	10.15	93.11
	6	4.5	2.21	[0_2/(0,90)]	11.66	121.32
	6	3	4.53	[0_4/$(0,90)_2$]	13.52	188.68

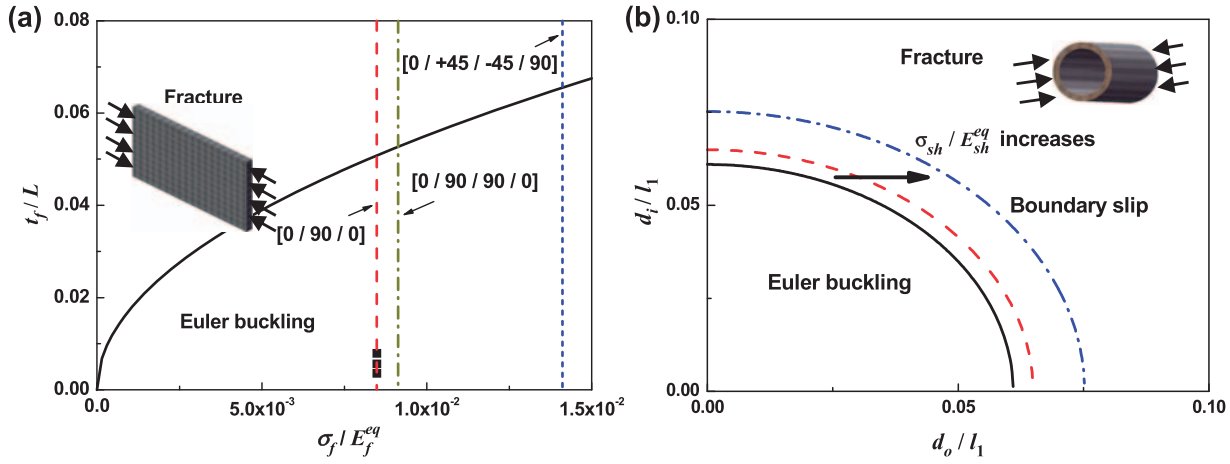

Figure 3. Failure mechanism maps for composite elements in axial compression: (a) laminated face sheet; (b) laminated shell.

Note that the boundaries for FC-SB and FW-SB are different for CPLs with different layups. Consider the composite design space as the region between the solid black curve ([$(0,90)_2$]) and the dashed blue curve ([0_4/$(0,90)_2$]) in Figure 4(d). If the selected geometry lies in this region, varying the truss layups can alter the failure mode. For example, two hollow CPL sandwich columns with equivalent dimensions are plotted as a single point (marked as a black dot), but if the truss lay-ups are [0_2/(0,90)] and [0_4/$(0,90)_2$], different failure modes will occur. The ability to tailor the truss properties distinguishes hollow CPLs from their counterparts. Analytical predictions based on classical laminate plate theory can greatly expand the designing space for CPL cores, but will not be discussed here.

Experiments

Fabrication

All-composite pyramidal lattice sandwich columns with hollow trusses were manufactured using the thermal expansion molding method, described elsewhere in detail.[12] The molds and embedding process are shown in Figure 5. Both unidirectional (3234/T700) and fabric prepreg (3234/G803, Beijing Institute of Aeronautical Materials, China) were used as parent materials in the present study. The stacking sequence of face sheets in all the tested specimens was $[0/90/0]_n$. The tube ends were embedded into the face sheets to enhance adhesion and mechanical interlocking (Figure 5(b)). Compression tests for the laminated face sheets cut from sandwich specimens yielded an equivalent elastic modulus E_f^{eq} of 41.2 GPa and a crushing strength σ_f of 135.8 MPa.

To encompass all the failure modes identified above and explore the practical limits of the analytical methods developed here, three sets of hollow CPL sandwich columns were designed and fabricated with different face-sheet thicknesses t_f and inner diameters d_i of hollow trusses. These are summarized in Table 2 and plotted as discrete points in Figure 4(a) to (c). Each specimen consisted of 2×4 cells with fixed column length $L = 200$ mm and core geometry ($d_o = 6$ mm, $l_1 = 19.8$ mm, $\omega = 45°$, and $l_2 = 15$ mm). Note that the bending-dominated macro-Euler buckling could not

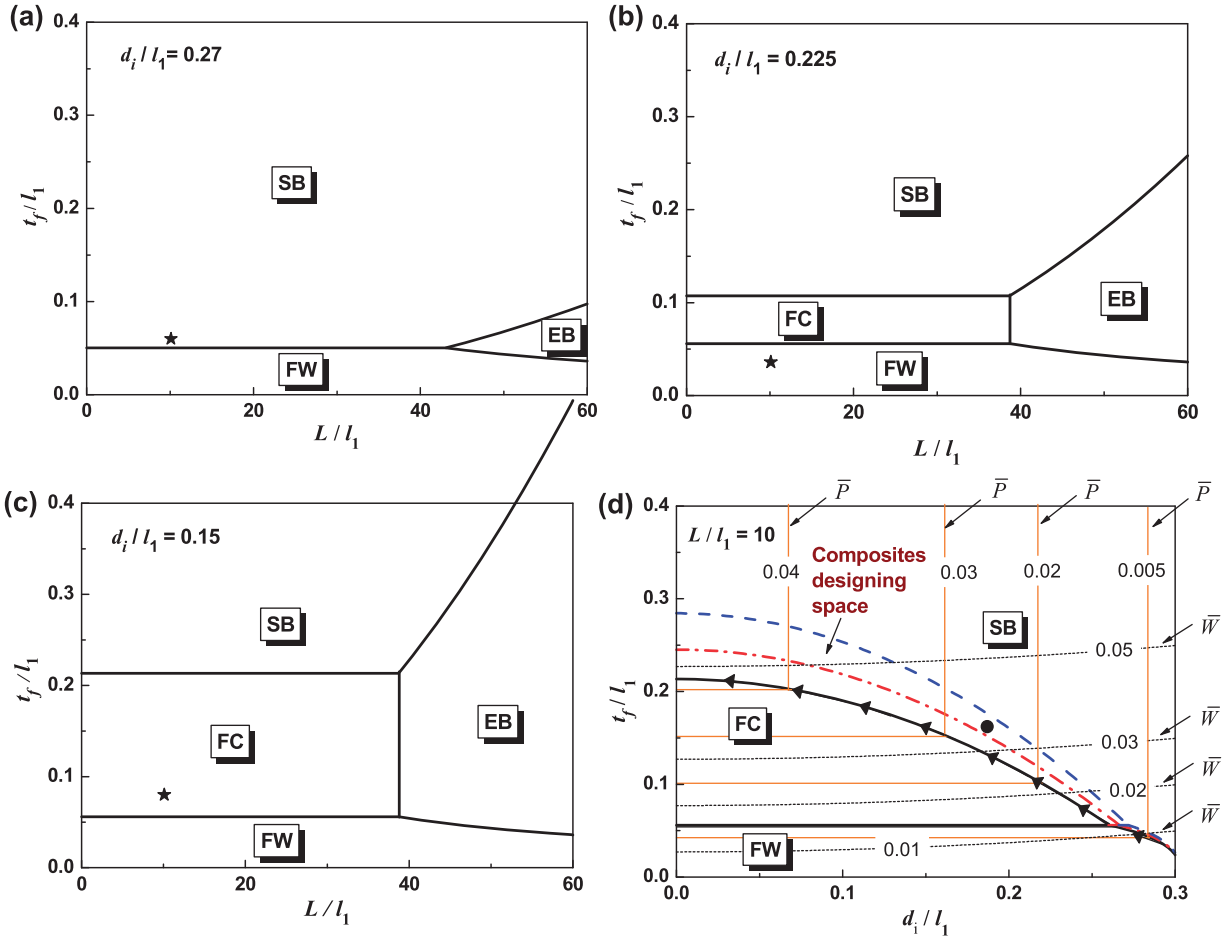

Figure 4. Failure mechanism maps for end compressed hollow CPL sandwich columns. In Figure d, the 'composites designing space' corresponds to the area among different boundary lines for CPLs with different lay-ups, and the arrows trace the path of optimum designs with increasing weight.
CPL: composite pyramidal lattice; SB: shear buckling; FW: face sheet wrinkling; FC: face sheet crushing; EB: Euler buckling.

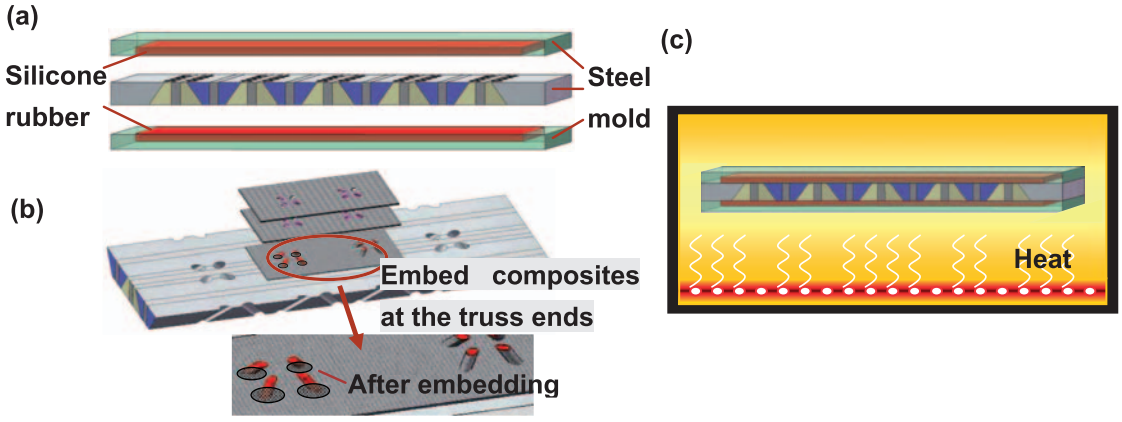

Figure 5. Illustration of the fabrication technique for hollow CPL sandwich columns: (a) the molds, (b) the embedding process and (c) curing. For details see Yin et al.[12] CPL: composite pyramidal lattice.

Table 2. Summary of the geometries employed in edgewise compression tests along with the predicted and measured failure loads and collapse modes.

Specimen	Number of ply in face sheet	L (mm)	w (mm)	t_f (mm)	d_i (mm)	Predicted failure mode	Predicted load (kN)	Measured load (kN)
A	6	199.32	99.81	0.71	4.5	FW	7.90	6.5
						FC	19.24	
						SB	57.43	
B	12	198.91	100.14	1.58	3	FW	87.41	38.12
						FC	42.91	
						SB	114.63	
C	9	200.2	101.2	1.12	5.4	FW	31.46	11.29
						FC	30.78	
						SB	19.01	

SB: shear buckling; FW: face sheet wrinkling; FC: face sheet crushing.

be achieved with the designs used here. A summary of the geometrical parameters of the tested specimens are listed in Table 2, along with the measured and predicted loads and failure modes.

Measurements

A low-viscosity epoxy adhesive was applied to the specimen ends and cured at room temperature for 1 h. The ends were then clamped tightly in fixtures, as shown in Figure 1(a). Compression tests were performed on hollow CPL sandwich panels at a displacement rate of 1 mm/min using a load frame (AG-250I). At least two specimens were tested for each geometry.

Face sheet wrinkling. For specimen A (6 plies in face sheet, $d_i = 4.5$ mm), the predicted and observed failure modes were face wrinkling (FW), plotted as the dot in Figure 4(b). The measured load–displacement curve is shown in Figure 6(a), and the corresponding photographs are presented in Figure 6(b). The load increases almost linearly until the peak load is reached. As the deflection of sandwich column increased, node rupture and face sheet delamination near the embedded truss ends was observed, leading to the fracture of face sheets. The predicted failure load (wrinkling) for specimen A is about 18% greater than the measured value (Table 2). This difference can be attributed to imperfections in the manufactured composite specimens, including defects introduced by embedding truss ends into the face sheets.

Face sheet crushing. Face sheet crushing can occur when the core is sufficiently strong and the face sheets are not ultra-thin, as in specimen B (Table 2). The measured compression response of specimen B (12 plies in face sheet, $d_i = 3$ mm, denoted by the dot in Figure 4(c)) is shown in Figure 7(a), along with the corresponding photographs in Figure 7(b). The peak load occurred at an axial displacement of $\sim$1.5 mm, followed by a sharp load drop (point II). Delamination was observed in the face sheets at the sites where truss ends were embedded, and followed by fracture (fiber micro-buckling) in close proximity. The observed failure mode is consistent with the mode predicted in the Appendix. Note that the delamination strength was limited by the insertion of truss ends into the face sheets, all of which were embedded in the same layer (as shown in Figure 5(b)). The increasing of delamination strength could be achieved by staggering the interplay sites at which the trusses insert.

Shear buckling. Shear buckling is the probable failure mode when the pyramidal core is relatively weak, and specimen C (9 face sheet plies, $d_i = 5.4$ mm, shown as the black dot in Figure 4(a)) was designed to investigate this failure mode. The measured response and collapse behavior are presented in Figure 8(a) and (b). The onset of shear buckling (point II in Figure 8(a)) occurred before the peak collapse load, which was associated with further bending of the hollow CPL sandwich columns. Node rupture was observed at displacements well beyond the peak load (point IV in Figure 8(a)). The stress state that develops in the core resembles shear loading when shear buckling happens, with two trusses in tension and two in compression. Thus, the shear strength of the CPL apparently affects the final peak load, which has also been clarified by Li.[9]

Shear buckling will continue to be the dominant failure mode even if the face sheet thickness increases, (e.g. by increasing to 12 plies), provided the hollow truss dimensions remain unchanged. For example,

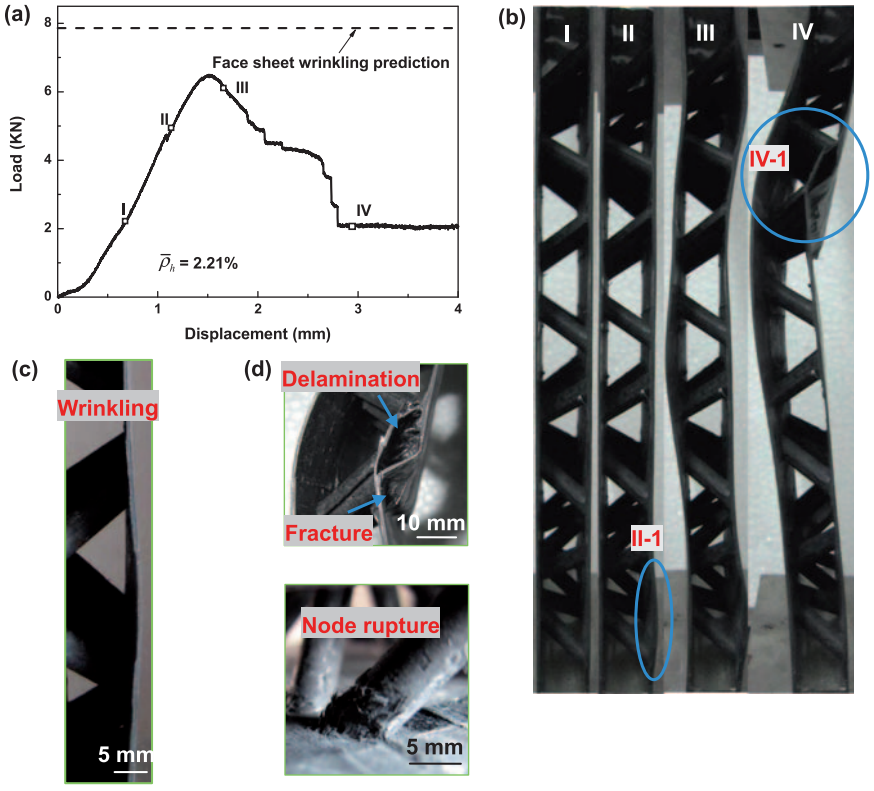

Figure 6. (a) Compressive response of specimen A; (b) photographs of the deformation history and corresponding failure modes of specimen in (a); (c) enlarged figure for II-1; (d) enlarged figure for IV-1.

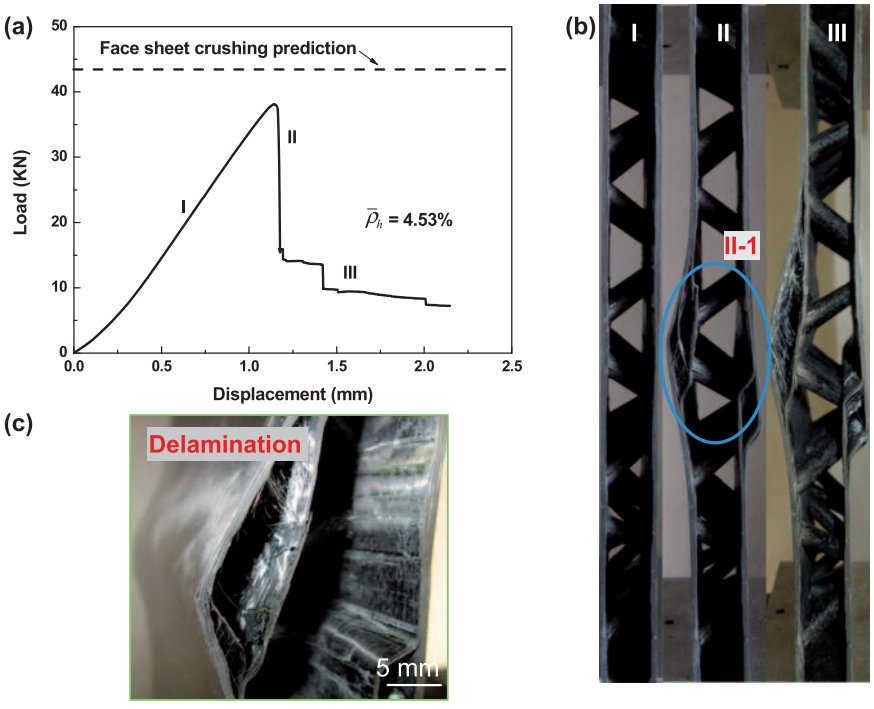

Figure 7. (a) Compressive response of specimen B; (b) photographs of the deformation history. Delamination occurred as one of micro-failure modes for face sheet crushing; (c) enlarged figure for II-1.

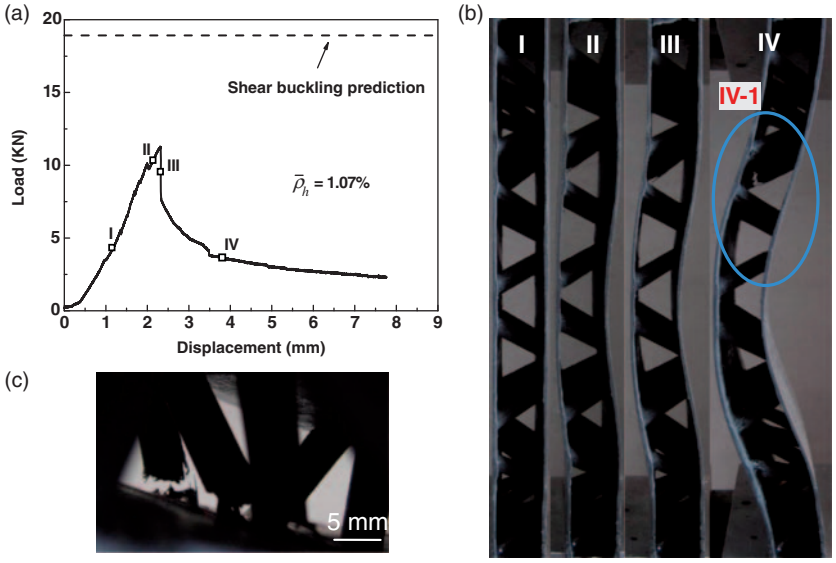

Figure 8. (a) Compressive response of specimen C; (b) photographs of the deformation history; (c) enlarged figure for IV-1. Note that Euler buckling was impossible due to the short column length employed.

comparison with specimen B, which features relatively strong face sheets and core (12 plies in face sheet, $d_i = 3$ mm), shows that the geometry of the lower-order laminated shell, which determines the relative density of the hollow CPL, controls the collapse mechanism of the sandwich columns. Note that the measured peak stress tends to be about 40% less than the predicted value, with some consistency. This discrepancy is attributed largely to fabrication defects, some of which are unavoidable, and none of which is accounted for in the model.

Minimum weight design

We would like to evaluate the load-carrying capacity of an optimized hollow CPL sandwich column in end compression by comparing with other competing structures at the same weight. In the optimal design, we need to select the geometries of both trusses and face sheets. The structural load index for an end-compressed sandwich column is $\bar{P} \equiv P/(\sigma_f w L)$, and the dimensionless weight $\bar{W}$ is given by

$$\bar{W} \equiv W/(\rho_{cf} w L^2) = 2\frac{t_f}{L} + \frac{\pi l_1 \left(d_o^2 - d_i^2\right)}{L\left(\sqrt{2} l_1 \cos\omega + 2 l_2\right)} \qquad (2)$$

where ρ_{cf} is the density of the parent carbon fiber composites and the difference in density between the face sheets and the hollow trusses is neglected. Thus, the contours of $\bar{P}$ and $\bar{W}$ are added into Figure 4(d). The arrows along the boundaries of the collapse domains indicate the path of optimal designs that maximize the peak load at a given weight. The relationship between $\bar{P}$ and $\bar{W}$ for an optimized hollow CPL structure can be expressed as

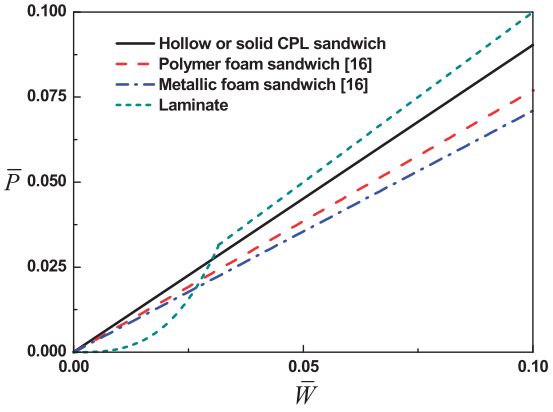

Figure 9. Structural efficiency of sandwich columns with hollow CPL core in end compression, compared with those with solid CPL core, polymer foam, metallic foam and solid laminate. CPL: composite pyramidal lattice.

$$\frac{\bar{P}}{\bar{M}} \equiv \frac{2}{2 + 16\sigma_f / E_{sh}} \qquad (3)$$

The realistic values of $\bar{P}$ for an optimized structure are assumed to collapse by combining face sheet wrinkling, crushing and shear buckling. The structural efficiency is defined as the peak load to weight ratio, and then the load index of the optimized hollow CPL sandwich column in end compression is plotted as a function of the minimum weight in Figure 9.

Structural efficiencies of sandwich columns with solid CPL core, polymer foam, aluminum foam and solid laminate (face sheet) are included in Figure 9 and compared with hollow CPL sandwich column. Structural efficiency of CPL core sandwich columns with either hollow or solid trusses is the same, which means the truss type has no effect on the structural performance in end compression. The sandwich column with hollow CPL core is about 17% and 21% lighter at the same load-carrying capacity than columns with polymer foam core and metallic foam core, respectively. Consider a laminate in end compression, and the failure mechanism has already been constructed in Figure 3(a). For $\bar{P} < 0.03$, Euler buckling dominates the failure. After the comparison, we can conclude that for the regime $\bar{P} < 0.02$, the sandwich columns are significantly lighter than solid laminate.

Conclusions

The in-plane compressive response of hollow CPL core sandwich panels was investigated experimentally and analytically from a hierarchical perspective. Compressive end-loading of sandwich columns resulted in the shear-like loading of the core, with two trusses in tension and the other two ones in compression. Collapse mechanism maps were constructed for both the composite components (i.e. face sheets and hollow trusses) and the hollow CPL sandwich structures. Observations revealed that the failure mode for flat laminates depends primarily on the geometrical parameter t_f/L, while altering the stacking sequence within the composite tube trusses can produce a transition between failure modes. For composite sandwich columns, these maps illustrate that failure mechanisms in end compression can be controlled by altering the properties of trusses of the hollow CPL core without even varying the dimensions of the sandwich structure.

For sandwich columns, three competing failure modes were observed in end compression tests: face sheet wrinkling, face sheet crushing, and shear macrobuckling (Euler buckling was not observed because of the laboratory equipment limitation for specimen length). The measured collapse loads followed the predicted trends and dependences, although a difference of nearly 40% was observed in the shear buckling case. These differences were attributed primarily to defects in the sample preparation and the practice of embedding trusses into face sheets.

The minimum weight design of the sandwich column with hollow CPL core in end compression was carried out, and the structural efficiency of an optimized structure was also compared with other columns. The optimal selection of sandwich core construction depended upon the required load index. In end compression, the sandwich column with hollow CPL core was as efficient as that with solid CPL core, and about 17% and 21% lighter than columns with polymer foam core and metallic foam core at the same load-carrying capacity, respectively. Also, the sandwich columns are significantly lighter than solid laminate for the regime $\bar{P} < 0.02$.

Conflict of interest

None declared.

Funding

This work was supported by NSFC (90816024 and 10872059), 973 Program (No. 2011CB610303). S.N. gratefully acknowledges support from the Gill Composites Center. S.Y. also acknowledges the support of Most Potential New Scholar Prize awarded by Ministry of Education in China (AUDQ1010000511) and the support from China Scholarship Council (CSC) during the visit at University of Southern California.

References

1. Evans AG, Hutchinson JW, Fleck NA, et al. The topological design of multifunctional cellular metals. *Prog Mater Sci* 2001; 46(3–4): 309–327.
2. Queheillalt DT and Wadley HNG. Cellular metal lattices with hollow trusses. *Acta Mater* 2005; 53(2): 303–313.
3. Queheillalt DT and Wadley HNG. Pyramidal lattice truss structures with hollow trusses. *Mater Sci Eng A* 2005; 397(1–2): 132–137.
4. Kooistra GW, Deshpande V and Wadley HNG. Hierarchical corrugated core sandwich panel concepts. *J Appl Mech* 2007; 74(2): 259–268.
5. Dharmasena KP, Queheillalt DT, Wadley HNG, et al. Dynamic compression of metallic sandwich structures during planar impulsive loading in water. *Eur J Mech A-Solids* 2010; 29(1): 56–67.
6. Dharmasena KP, Queheillalt DT, Wadley HNG, et al. Dynamic response of a multilayer prismatic structure to impulsive loads incident from water. *Int J Impact Eng* 2009; 36(4): 632–643.
7. Yungwirth CJ, Wadley HNG, O'Connor JH, et al. Impact response of sandwich plates with a pyramidal lattice core. *Int J Impact Eng* 2008; 35(8): 920–936.
8. McShane GJ, Stewart C, Aronson MT, et al. Dynamic rupture of polymer-metal bilayer plates. *Int J Solids Struct* 2008; 45(16): 4407–4426.
9. Li M, Wu LZ, Ma L, et al. Structural response of all-composite pyramidal truss core sandwich columns in end compression. *Compos Struct* 2011; 93(8): 1964–1972.
10. Xiong J, Ma L, Wu LZ, et al. Fabrication and crushing behavior of low density carbon fiber composite pyramidal truss structures. *Compos Struct* 2010; 92(11): 2695–2702.
11. Wang B, Wu LZ, Ma L, et al. Mechanical behavior of the sandwich structures with carbon fiber-reinforced pyramidal lattice truss core. *Mater Des* 2010; 31(5): 2659–2663.

12. Yin S, Wu LZ, Ma L, et al. Pyramidal lattice sandwich structures with hollow composite trusses. *Compos Struct* 2011; 93(12): 3104–3111.
13. Russell BP, Deshpande VS and Wadley HNG. Quasistatic deformation and failure modes of composite square honeycombs. *J Mech Mater Struct* 2008; 3(7): 1315–1340.
14. Finnegan K, Kooistra G, Wadley HNG, et al. The compressive response of carbon fiber composite pyramidal truss sandwich cores. *Int J Mater Res* 2007; 98(12): 1264–1272.
15. Yin S, Wu LZ, Ma L, et al. Hybrid truss concepts for carbon fiber composite pyramidal lattice structures. *Compos Part B-Eng* 2012; 43(4): 1749–1755.
16. Fleck NA and Sridhar I. End compression of sandwich columns. *Compos Part A-Appl Sci Manuf* 2002; 33(3): 353–359.
17. Cote F, Biagi R, Bart-Smith H, et al. Structural response of pyramidal core sandwich columns. *Int J Solids Struct* 2007; 44(10): 3533–3556.
18. Lakes R. Materials with structural hierarchy. *Nature* 1993; 361(6412): 511–515.
19. Xiong J, Ma L, Wu LZ, et al. Mechanical behavior and failure of composite pyramidal truss core sandwich columns. *Compos Part B-Eng* 2011; 42(4): 938–945.
20. Jones RM. *Mechanics of composite materials*, 2nd edn. New York: Taylor & Francis.
21. Zenkert D. *An introduction to sandwich construction*. Sheffield, UK: Engineering Materials Advisory Service, 1995.
22. Deshpande VS and Fleck NA. Collapse of truss core sandwich beams in 3-point bending. *Int J Solids Struct* 2001; 38(36–37): 6275–6305.

Appendix

Analytical predictions

Wrinkling of face sheets. The laminated face sheets of the sandwich column will readily wrinkle under compression loading as the face sheets are relatively thin. Wrinkling is the local short-wavelength elastic buckling of the face sheets between the nodes of attachment to the CPL. The wrinkling load of the CPL sandwich column can be expressed as

$$P_{fw} = \frac{2k^2\pi^2 D_f}{\left(\sqrt{2}l_1\cos\omega + l_2\right)^2} \tag{4}$$

where k depends on the constraint conditions between the CPL core and the face sheets, and we assume $k = 2$ due to the embedding process employed during fabrication (described in section 'Experiments').[12]

Crushing of face sheets. The carbon fiber composite face sheet is treated as an elastic solid that will crush when the axial compressive load reaches the crushing strength, denoted as σ_f. Consequently, the face sheet collapse load is obtained by setting the stress in the face sheets to the crushing strength and is expressed as

$$P_{fc} = 2\sigma_f t_f w \tag{5}$$

Euler buckling of hollow CPL sandwich column. Compressive loading of sandwich columns can also result in Euler buckling, as shown in Figure 2(c). The sandwich column is considered to be composed of built-in Euler columns, and the compressive collapse load is specified by

$$P_{eb} = \frac{4\pi^2 D_{sand}}{L^2} \tag{6}$$

where the equivalent flexural rigidity of the sandwich panel, D_{sand}, is given by

$$D_{sand} = \frac{1}{2}E_f^{eq} w t_f \left(t_f + t_c\right)^2 + \frac{1}{6}E_f^{eq} w t_f^3 + \frac{1}{12}E_c w t_c^3 \approx \frac{1}{2}E_f^{eq} w t_f t_c^2 \tag{7}$$

Here, w is the width of the sandwich column, t_f is the face sheet thickness, t_c is the pyramidal core height, and E_c is the elastic modulus of the hollow CPL.

Shear buckling of hollow CPL sandwich column. The fourth failure mode considered is shear buckling, shown schematically in Figure 2(d). The core shear buckling load P_{sb} is set by the shear stiffness S of the CPL, as described by Zenkert,[21] and occurs at

$$P_{sb} = S = G_c w l_1 \sin\omega \tag{8}$$

where G_c is the shear modulus of the hollow CPL. The CPL shear modulus is independent of the loading direction,[22] and if the bending contribution of the hollow trusses is neglected, G_c is given by

$$G_c = \frac{1}{8}E_{sh}^{eq}\bar{\rho}_h \sin^2 2\omega \tag{9}$$

where E_{sh}^{eq} is the equivalent elastic modulus of the composite tube.